Journal of Computational Physics 229 (2010) 6071–6083

Contents lists available at ScienceDirect

Journal of Computational Physics

journal homepage: www.elsevier.com/locate/jcp

Using sensitivity derivatives for design and parameter estimation in an atmospheric plasma discharge simulation

Kyle J. Lange [a,*], W. Kyle Anderson [b]

[a] University of Victoria, Institute for Integrated Energy Systems, Victoria, BC V8W 2Y2, Canada
[b] University of Tennessee-Chattanooga, National Center for Computational Engineering, Chattanooga, TN 37403, USA

ARTICLE INFO

Article history:
Received 17 December 2009
Accepted 23 April 2010
Available online 4 May 2010

Keywords:
Plasma discharge
Sensitivity analysis
Uncertainty analysis
Adjoint
Direct differentiation
Optimization

ABSTRACT

The problem of applying sensitivity analysis to a one-dimensional atmospheric radio frequency plasma discharge simulation is considered. A fluid simulation is used to model an atmospheric pressure radio frequency helium discharge with a small nitrogen impurity. Sensitivity derivatives are computed for the peak electron density with respect to physical inputs to the simulation. These derivatives are verified using several different methods to compute sensitivity derivatives. It is then demonstrated how sensitivity derivatives can be used within a design cycle to change these physical inputs so as to increase the peak electron density. It is also shown how sensitivity analysis can be used in conjunction with experimental data to obtain better estimates for rate and transport parameters. Finally, it is described how sensitivity analysis could be used to compute an upper bound on the uncertainty for results from a simulation.

1. Introduction

Since the seminal work of Graves and Jensen [1], there have been numerous efforts to accurately simulate plasma discharges [2–8], which are used in a variety of applications including microelectronics manufacturing, lighting, and plasma display panels. Many of these simulations have been motivated by a need to better understand the underlying physics in plasma discharges. A variety of approaches have been used including particle-in-cell methods, fluid simulations, and hybrid models.

There have also been efforts to use simulations of plasma discharges to perform parameter studies, or qualitative sensitivity analysis [9–12]. The typical approach that is used is to change a given parameter for a plasma discharge (e.g. pressure, temperature) and run the simulation with the new value for the parameter to see what changes have taken place. This can provide valuable information about the sensitivity of the plasma behavior to various parameters and can be useful for optimization or design. However, this can be computationally expensive, as the simulation must be run every time that a parameter is changed. In addition, although this approach can provide qualitative information, it does not yield any quantitative sensitivity derivatives.

Quantitative sensitivity analysis, using finite differences, complex perturbations, direct differentiation or adjoint, can be used to compute numerical sensitivity derivatives of cost functions to given design variables. In recent years, sensitivity derivatives have been computed for unsteady time-dependent problems [13–16]. In a previous paper, the authors used time-dependent sensitivity analysis to compute sensitivity derivatives for a one-dimensional low-pressure helium discharge simulation [17], where only electrons and helium monomer ions were modeled. To the knowledge of the authors, this was the first time that quantitative sensitivity derivatives were computed for a plasma discharge simulation.

* Corresponding author.
E-mail addresses: klange@uvic.ca (K.J. Lange), kyle-anderson@utc.edu (W.K. Anderson).

0021-9991/$ - see front matter © 2010 Elsevier Inc. All rights reserved.
doi:10.1016/j.jcp.2010.04.038

High pressure glow (HPG) discharge systems are more economical than low pressure discharge systems since no vacuum pump is needed. For this reason, there has been a plethora of research done on HPG plasmas in the last decade. Many applications of HPG discharges have been reported including etching and deposition [18,19], decontamination of chemical and biological warfare agents [20], the treatment of dental cavities [21], and as a means for sterilization [22,23].

In the current paper, quantitative sensitivity analysis has been applied to a one-dimensional high-pressure helium/nitrogen glow discharge simulation. The paper is organized in the following manner. Section 2 describes the equations and boundary conditions used in the simulation. Section 3 describes the numerical methods and discretization used to obtain a periodic solution. Section 4 presents a review of the different methods that can be used to compute sensitivity derivatives. Section 5 presents the verification of the sensitivity derivatives and several applications of sensitivity analysis for a plasma discharge simulation. The paper is summarized in Section 6.

2. Description of the model

2.1. Governing equations

A one-dimensional fluid model accounting for ten chemical species is used to simulate a plasma discharge that was modeled in a previous work [11]. Note that this model does not take into account effects from non-Maxwellian particle distributions. The discharge gas is assumed to be predominantly helium with a very small amount of nitrogen. It is assumed that the nitrogen has an impurity mole fraction of 5×10^{-7}. The following chemical species are used in the model: electrons (e), helium atoms (He), monomer helium ions (He^+), dimer helium ions (He_2^+), monomer helium metastables (He^*), dimer helium metastables (He_2^*), monomer nitrogen atoms (N), dimer nitrogen molecules (N_2), monomer nitrogen ions (N^+), and dimer nitrogen ions (N_2^+). These equations are summarized below:

$$\frac{\partial n_i}{\partial t} + \frac{\partial \Gamma_i}{\partial x} = \dot{G}_i, \tag{1}$$

$$\Gamma_i = -D_i \frac{\partial n_i}{\partial x} + \mu_i n_i E, \tag{2}$$

$$\frac{\partial}{\partial t}\left(\frac{3}{2} n_e k_B T_e\right) + \frac{\partial Q_e}{\partial x} = -e\Gamma_e E - e\sum_{j=1}^{r} \Delta E_j^e G_j - 3 n_e k_B \frac{m_e}{m_{He}} (T_e - T_{gas})\overline{\nu_e}, \tag{3}$$

$$Q_e = -\eta_e \frac{\partial T_e}{\partial x} + \frac{5}{2} k_B T_e \Gamma_e, \tag{4}$$

$$\epsilon_0 \frac{\partial}{\partial t}\left(\frac{\partial V}{\partial x}\right) = -j_{tot} + \sum_{i=1}^{i=n_s} e Z_i \Gamma_i, \tag{5}$$

$$E = -\frac{\partial V}{\partial x}. \tag{6}$$

Eq. (1) is the continuity equation which is used for each species density. Eq. (2) expresses the flux for each species with the drift–diffusion approximation. Eq. (3) is the electron energy equation, while the electron energy flux is expressed in Eq. (4). The total current in the discharge is specified using Eq. (5) and the electric field is expressed in Eq. (6).

Bringing all the equations together allows one to express them in conservative form as

$$\frac{\partial \mathbf{Q}}{\partial t} + \nabla \cdot \mathbf{F} = \mathbf{S}, \tag{7}$$

where **Q** represents the time-dependent terms in the governing equations, **F** represents the flux terms in the governing equations and **S** represents the source terms in the governing equations.

2.2. Transport properties

The values for transport properties are found in the literature [24–26] and are summarized in a previous work [11]. Diffusion coefficients can be computed from reduced diffusion coefficients as $D_k = D_k'\left(\frac{760}{p}\right)$, while mobilities can be computed from reduced mobilities as $\mu_k = \mu_k'\left(\frac{760}{p}\right)$, where p is measured in Torr.

The values for reduced diffusion coefficients and reduced mobilities are shown in Table 1.

2.3. Chemical reactions

The values used for reaction rate coefficients and other coefficients in determining production and destruction of chemical species are found in previous works [6,27–29] and are compiled in a previous work [11]. The reactions are summarized in Table 2. The electron energy gains and losses for given reactions are shown in Table 3.

Table 1
Transport properties for species in plasma discharge model.

Species	$D'_k(\mathrm{m}^2/\mathrm{sec},\ \mathrm{K},\ \mathrm{eV})$	$\mu'_k(\mathrm{m}^2/\mathrm{V}-\mathrm{sec})$
e	$1.737\times10^{-1}\left(\frac{T_e}{17{,}406}\right)$	$-1.132\ \times10^{-1}$
He^+	5.026×10^{-5}	1.482×10^{-3}
He_2^+	$8{,}148\times10^{-5}$	2.403×10^{-3}
N^+	9.710×10^{-5}	2.863×10^{-3}
N_2^+	1.015×10^{-4}	2.993×10^{-3}
He^*	4.116×10^{-4}	–
He_2^*	2.029×10^{-4}	–
He	4.116×10^{-4}	–
N	1.955×10^{-4}	–
N_2	1.075×10^{-4}	–

Table 2
Reaction mechanisms used in plasma discharge model.

Reaction	Numerical model (m, molecules, sec, K)
$e + He \rightarrow He^* + e$	$G_1 = (2.308\times10^{-16})n_e n_{He} T_e^{0.31} e^{-2.297\times10^5/T_e}$
$e + He^* \rightarrow He + e$	$G_2 = (1.099\times10^{-17})n_e n_{He^*} T_e^{0.31}$
$e + He \rightarrow He^+ + 2e$	$G_3 = (2.584\times10^{-18})n_e n_{He} T_e^{0.68} e^{-2.854092\times10^5/T_e}$
$e + He^* \rightarrow He^+ + 2e$	$G_4 = (4.661\times10^{-16})n_e n_{He^*} T_e^{0.6} e^{-5.546\times10^4/T_e}$
$e + He_2^* \rightarrow He_2^+ + 2e$	$G_5 = (1.268\times10^{-18})n_e n_{He_2^*} T_e^{0.71} e^{-3.945\times10^4/T_e}$
$e + He_2^+ \rightarrow He^* + He$	$G_6 = (5.386\times10^{-13})n_e n_{He_2^+} T_e^{-0.5}$
$He^* + He^* \rightarrow He^+ + He + e$	$G_7 = (2.7\times10^{-16})n_{He^*} n_{He^*}$
$He^* + 2He \rightarrow He_2^* + He$	$G_8 = (1.3\times10^{-45})n_{He^*} n_{He} n_{He}$
$He^+ + 2He \rightarrow He_2^+ + He$	$G_9 = (1.0\times10^{-43})n_{He^+} n_{He} n_{He}$
$He^* + N_2 \rightarrow N_2^+ + He + e$	$G_{10} = (7.0\times10^{-17})n_{He^*} n_{N_2}$
$He_2^* + N_2 \rightarrow N_2^+ + 2He + e$	$G_{11} = (7.0\times10^{-17})n_{He_2^*} n_{N_2}$
$He^+ + N_2 \rightarrow N_2^+ + He$	$G_{12} = (5.0\times10^{-16})n_{He^+} n_{N_2}$
$He^+ + N_2 \rightarrow N^+ + N + He$	$G_{13} = (7.0\times10^{-16})n_{He^+} n_{N_2}$
$He_2^+ + N_2 \rightarrow N_2^+ + 2He$	$G_{14} = (5.0\times10^{-16})n_{He_2^+} n_{N_2}$
$He_2^+ + N_2 \rightarrow N^+ + N + 2He$	$G_{15} = (7.0\times10^{-16})n_{He_2^+} n_{N_2}$
$2e + N_2^+ \rightarrow N_2 + e$	$G_{16} = (5.651\times10^{-39})n_e n_e n_{N_2^+} T_e^{-0.8}$
$e + N_2^+ \rightarrow N + N$	$G_{17} = (2.540\times10^{-12})n_e n_{N_2^+} T_e^{-0.5}$
$e + N_2 \rightarrow N + N + e$	$G_{18} = (1.959\times10^{-12})n_e n_{N_2} T_e^{-0.7} e^{-1.132\times10^5/T_e}$
$e + N \rightarrow N^+ + 2e$	$G_{19} = (8.401\times10^{-11})n_e n_N e^{-1.682\times10^5/T_e}$
$e + N_2 \rightarrow N_2^+ + 2e$	$G_{20} = (4.483\times10^{-13})n_e n_{N_2} T_e^{-0.3} e^{-1.81\times10^5/T_e}$

Table 3
Electron energy gains and losses used in plasma discharge model.

Reaction	Energy gain or loss (eV)
$e + He \rightarrow He^* + e$	$\Delta E_1^e = 19.8$
$e + He^* \rightarrow He + e$	$\Delta E_2^e = -19.8$
$e + He \rightarrow He^+ + 2e$	$\Delta E_3^e = 24.6$
$e + He^* \rightarrow He^+ + 2e$	$\Delta E_4^e = 4.78$
$e + He_2^* \rightarrow He_2^+ + 2e$	$\Delta E_5^e = 3.4$
$He^* + He^* \rightarrow He^+ + He + e$	$\Delta E_7^e = -15.0$
$e + N_2 \rightarrow N + N + e$	$\Delta E_{18}^e = 9.757$
$e + N \rightarrow N^+ + 2e$	$\Delta E_{19}^e = 14.5$
$e + N_2 \rightarrow N_2^+ + 2e$	$\Delta E_{20}^e = 15.6$

2.4. Boundary conditions

The fluxes for the electrons, metastable species and monomer nitrogen atoms at the boundaries are assumed to be kinetically limited thermal fluxes which are directed outward. Thus, at the left boundary, these fluxes are negative, while at the right boundary, these fluxes are positive. The ion fluxes are assumed to be mobility limited. One change that has been made

to the model used by Yuan and Raja is that the mobility limited ion fluxes are only computed when the electric field is accelerating them towards the boundaries. Otherwise these fluxes are set equal to zero. This ensures that additional helium and nitrogen particles are not added to the simulation through the mobility flux boundary conditions.

Recombination is assumed to occur at the boundaries, and all helium and nitrogen particles are assumed to return to the discharge as either He or N_2 particles. The electron temperature is set equal to 0.5 eV at each boundary. At one boundary of the discharge, the potential is grounded. At the opposite boundary, the voltage is computed using the specified boundary fluxes of the charged particles. It is assumed that there is no secondary electron emission at the boundaries. The boundary conditions for each particle species are summarized in Table 4.

3. Numerical method

3.1. Mesh discretization

The domain is discretized into control volumes by distributing mesh points across the domain according to an algorithm that clusters the points close to the boundaries, which has been used in previous simulations [30]. The faces of the control volumes are designated to be halfway in between the mesh points except for at the boundaries, where the mesh points are coincident with the cell faces. The mesh setup is shown in Fig. 1.

The spatial discretization is represented with subscripts by the index k. Integer values such as k and $k+1$ denote a value within a given cell. Half-integer values such as $k+\frac{1}{2}$ and $k-\frac{1}{2}$, denote the values at cell faces. The distance between points k and $k+1$ is denoted as Δx_k while the distance between faces $k+\frac{1}{2}$ and $k-\frac{1}{2}$, the cell volume, is represented by Ω_k.

3.2. Spatial discretization

A finite volume approach is used to discretize the equations. A staggered mesh and non-staggered mesh approach have each been implemented for the simulation. Although both approaches yield the same results, only results for the staggered grid approach are presented here. In this approach, the values for the potential V are stored at cell faces, and values for the remaining variables (species densities and electron energy) are stored at cell centers. For M control volumes, there are M unknowns for each species densities and the electron energy, with $M+1$ unknowns for the voltage. However, since the voltage is grounded at one electrode, and its value does not change during the simulation, this results in M unknowns for the voltage, making this a straightforward system of equations to solve since each of the M control volumes has 12 unknown variables associated with it, corresponding to the 10 particle species densities, the electron energy and the voltage.

Applying a finite volume method to the governing equations and applying Green's theorem to Eq. (7) results in the following discretization:

$$\Omega_k \frac{\partial \mathbf{Q}_k}{\partial t} + \mathbf{F}_{k+\frac{1}{2}} - \mathbf{F}_{k-\frac{1}{2}} = \Omega_k \mathbf{S}_k. \tag{8}$$

Table 4
Boundary conditions for species in plasma discharge model.

Species	Boundary condition
e	$\Gamma_e = \mp\frac{1}{4} n_e \sqrt{\frac{8 k_B T_e}{\pi m_e}}$
He^+	$\Gamma_{He^+} = \begin{cases} \mu_{He^+} n_{He^+} E & \text{if } \vec{E}\cdot\hat{n} > 0 \\ 0 & \text{if } \vec{E}\cdot\hat{n} \leqslant 0 \end{cases}$
He_2^+	$\Gamma_{He_2^+} = \begin{cases} \mu_{He_2^+} n_{He_2^+} E & \text{if } \vec{E}\cdot\hat{n} > 0 \\ 0 & \text{if } \vec{E}\cdot\hat{n} \leqslant 0 \end{cases}$
He^*	$\Gamma_{He^*} = \mp\frac{1}{4} n_{He^*} \sqrt{\frac{8 k_B T_{gas}}{\pi m_{He^*}}}$
He_2^*	$\Gamma_{He_2^*} = \mp\frac{1}{4} n_{He_2^*} \sqrt{\frac{8 k_B T_{gas}}{\pi m_{He_2^*}}}$
N	$\Gamma_N = \mp\frac{1}{4} n_N \sqrt{\frac{8 k_B T_{gas}}{\pi m_N}}$
N^+	$\Gamma_{N^+} = \begin{cases} \mu_{N^+} n_{N^+} E & \text{if } \vec{E}\cdot\hat{n} > 0 \\ 0 & \text{if } \vec{E}\cdot\hat{n} \leqslant 0 \end{cases}$
N_2^+	$\Gamma_{N_2^+} = \begin{cases} \mu_{N_2^+} n_{N_2^+} E & \text{if } \vec{E}\cdot\hat{n} > 0 \\ 0 & \text{if } \vec{E}\cdot\hat{n} \leqslant 0 \end{cases}$
He	$\Gamma_{He} = -(\Gamma_{He^+} + 2\Gamma_{He_2^+} + \Gamma_{He^*} + 2\Gamma_{He_2^*})$
N_2	$\Gamma_{N_2} = -\left(\frac{1}{2}\Gamma_{N^+} + \Gamma_{N_2^+} + \frac{1}{2}\Gamma_N\right)$

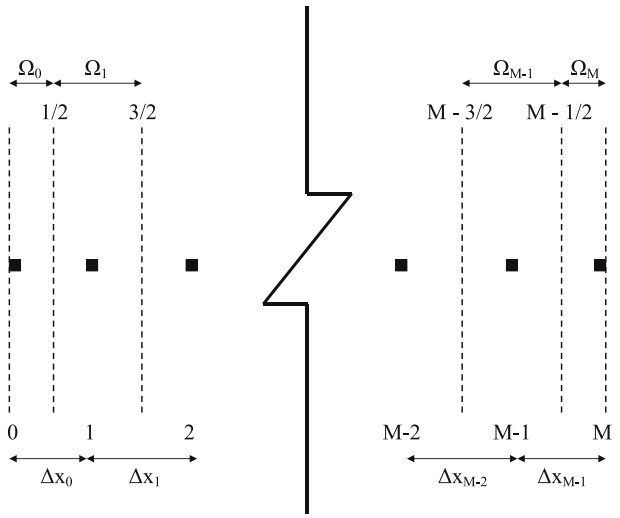

Fig. 1. Discretization of domain into M control volumes with $M + 1$ grid points.

The time derivatives and source terms are computed at the center of each control volume. Their contribution to the residual is computed by multiplying these terms by the length of the control volume. The fluxes are computed at each cell face.

For neutral and metastable particles, the flux is entirely diffusive and is discretized as

$$\Gamma_{i,k+\frac{1}{2}} = -D_i\left(\frac{n_{i,k+1} - n_{i,k}}{\Delta x_k}\right). \tag{9}$$

The logarithms of the charged particle densities and the electron energy are used as fundamental variables in the simulation, as was done in a previous work [17]. This is done because these quantities are inherently positive, and because second-order spatial accuracy in the finite volume scheme is achieved by extrapolating values from cell centers to cell faces. In regions where there are steep gradients, this extrapolation can lead to negative densities or a negative electron energy.

Thus, the charged particle flux at each face is computed as

$$\Gamma_{i,k+\frac{1}{2}} = -D_{i,k+\frac{1}{2}}\left(\frac{n_{i,k+1} - n_{i,k}}{\Delta x_k}\right) + \mu_i n_{i,k+\frac{1}{2}}\left(\frac{1}{2}(E_k + E_{k+1})\right). \tag{10}$$

In Eq. (10), $n_{i,k+\frac{1}{2}}$ is computed differently based on the sign of the electric field and the species charge. It is computed as

$$n_{i,k+\frac{1}{2}} = \begin{cases} \exp\left(Q_{i,k} + \frac{1}{2}\Delta x_k\left(\frac{\partial Q}{\partial x}\right)_{i,k}\right) & \text{if } Z_i E \geqslant 0 \\ \exp\left(Q_{i,k+1} - \frac{1}{2}\Delta x_k\left(\frac{\partial Q}{\partial x}\right)_{i,k+1}\right) & \text{if } Z_i E < 0 \end{cases}. \tag{11}$$

The electric field in Eq. (10) is computed as

$$E_k = -\frac{\left(V_{k+\frac{1}{2}} - V_{k-\frac{1}{2}}\right)}{\Omega_k}. \tag{12}$$

Note that the convective flux discretization at the face is the same for the cell to the right of the face and the cell to the left of the face. For one cell, this flux is subtracted from the residual and for the other, the flux is added to the residual. In this way, the total particle flux is conserved in the simulation.

The current conservation equation, which is different from the other equations in that it involves the time derivative of a spatial derivative, is discretized as

$$\frac{\partial}{\partial t}\left(\frac{V_{k+\frac{1}{2}} - V_{k-\frac{1}{2}}}{\Omega_k}\right)\Omega_k = -j_{tot}\Omega_k + \sum_{i=1}^{i=n_s} eZ_i\left(\frac{1}{2}\Delta x_k \Gamma_{i,k+\frac{1}{2}} + \frac{1}{2}\Delta x_{k-1}\Gamma_{i,k-\frac{1}{2}}\right). \tag{13}$$

Each equation is non-dimensionalized for stable and efficient computation. They are non-dimensionalized in a way that is similar to previous computational models [7,30].

3.3. Temporal discretization

All time derivatives are computed using a second-order backwards difference formula as

$$\left(\frac{\partial a}{\partial t}\right)_k^n = \frac{3a_k^n - 4a_k^{n-1} + a_k^{n-2}}{2\Delta t}, \tag{14}$$

where Δt is the time step used in the simulation. A fully implicit method is used, meaning that all fluxes and source terms are evaluated at the current time step n.

3.4. Solving the system of equations

Newton's method is used to solve the discretized linear equations at each time step. The Newton iterations continue within a given time step until the norm of the residual in a given Newton iteration falls below a specified tolerance. This indicates that the updated value $\mathbf{Q}^n$ has been computed, and the solution is advanced to the next time step. This process is repeated until a periodic solution has been computed.

Newton's method requires the computation of the Jacobian matrix $\frac{\partial \mathbf{R}}{\partial \mathbf{Q}}$, which is the linearization of the residual vector $\mathbf{R}$ with respect to the variable vector $\mathbf{Q}$. The Jacobian matrix is computed analytically for computational efficiency. For this one-dimensional simulation with second-order spatial accuracy, the Jacobian matrix is block penta-diagonal. The problem is parallelized to run on multiple processors and uses GMRES [31] with an approximate ILU preconditioner [32].

To reduce the computational runtime of the simulation, initial approximations of the solution variables are computed at the beginning of each time step. The time derivative of each variable is computed using a third-order backwards difference as

$$\frac{dQ^{n-1}}{dt} = \frac{11Q^{n-1} - 18Q^{n-2} + 9Q^{n-3} - 2Q^{n-4}}{6\Delta t}. \tag{15}$$

The second and third derivatives of each variable are computed in a similar manner as:

$$\frac{d^2Q}{dt^2}^{n-1} = \frac{11\frac{dQ}{dt}^{n-1} - 18\frac{dQ}{dt}^{n-2} + 9\frac{dQ}{dt}^{n-3} - 2\frac{dQ}{dt}^{n-4}}{6\Delta t}, \tag{16}$$

$$\frac{d^3Q}{dt^3}^{n-1} = \frac{11\frac{d^2Q}{dt^2}^{n-1} - 18\frac{d^2Q}{dt^2}^{n-2} + 9\frac{d^2Q}{dt^2}^{n-3} - 2\frac{d^2Q}{dt^2}^{n-4}}{6\Delta t}. \tag{17}$$

An approximation to the variable at time step n is then computed using a Taylor series expansion along with Eqs. (15)–(17) as

$$Q^n \approx Q^{n-1} + \Delta t\left(\frac{dQ}{dt}\right)^{n-1} + \frac{\Delta t^2}{2}\left(\frac{d^2Q}{dt^2}\right)^{n-1} + \frac{\Delta t^3}{6}\left(\frac{d^3Q}{dt^3}\right)^{n-1}. \tag{18}$$

Using this approximation for the solution at the next time step has been shown to reduce the computational runtime by 60%.

4. Computing sensitivity derivatives

4.1. Perturbation methods

Perturbation methods rely on a perturbation in a design variable β to compute the sensitivity with regard to a cost function I. Using a Taylor series approximation, a sensitivity derivative can be computed using finite differences as

$$\frac{dI}{d\beta} = \frac{I(\beta + \Delta\beta) - I(\beta)}{\Delta\beta}. \tag{19}$$

This can be useful in some cases, but it is subject to cancellation error and can be sensitive to the size of the perturbation $\Delta\beta$. One way to avoid the cancellation error is to use a complex perturbation [33–35]. In this case, the entire computer code is converted to complex numbers and the design variable is perturbed in the complex plane, allowing the sensitivity derivative to be computed as the imaginary part of the computed cost function as

$$\frac{dI}{d\beta} = \mathrm{Imag}\left(\frac{I(\beta + i\Delta\beta)}{\Delta\beta}\right). \tag{20}$$

The cancellation error is eliminated in this case, but using complex numbers can significantly increase the computational load for a simulation. Both perturbation methods can compute a sensitivity derivative vector for multiple cost functions with respect to one design variable, but they suffer from the fact that the process must be repeated for each design variable.

4.2. Differentiation methods

Two different types of differentiation methods are used to compute sensitivity derivatives. The first method is forward mode direct differentiation [36], which can be used to compute the sensitivity derivatives of an unlimited number of cost functions with respect to one design variable. In direct differentiation, the sensitivity derivatives are computed as the solution advances in time.

The second method is the reverse mode adjoint method [37,38,14], which computes the sensitivity of one cost function to an unlimited number of design variables. In this case, after the periodic solution has been reached, the sensitivity derivatives are computed using solution values at each previous time step, going all the way back to the initial conditions.

Differentiation methods can be implemented continuously [39–41] or discretely [42–44]. The continuous sensitivity method differentiates the governing equations first with respect to the design variables, and then discretizes them, while a discrete sensitivity method discretizes the governing equations first and then differentiates them with respect to design variables. Discrete sensitivity methods are used in this work.

The algorithms for time-dependent sensitivity analysis have been expressed in previous papers [13,14,16,17] and are not reproduced here.

Direct differentiation does not require much storage because the necessary information can be overwritten as the algorithm proceeds. However, if there are multiple design variables, direct differentiation must be repeated for each design variable. Reverse mode adjoint requires more storage than forward mode direct differentiation since the solution vector must be stored or recomputed at every single time step in the solution process. This can be accomplished either by storing the solutions in memory or by writing out the solutions to a file. If there are multiple cost functions, reverse mode adjoint must be repeated for each cost function.

The additional work required for adjoint and direct differentiation is equivalent to an extra linear solve at each time step. In addition, for reverse mode adjoint, the transpose of the Jacobian matrix must be formed.

5. Computational results and discussion

The simulation is run on a 81 point grid. The design variables considered are the scalar components of the reaction rate coefficients for each of the 20 reactions ($k_1, k_2, \ldots, k_{20}$), the reduced mobilities and the diffusion coefficients for each species, the nitrogen impurity fraction f_N, the gas pressure p, the discharge gap length l, the rms current density j_{rms}, the frequency f, and the gas temperature T_{gas}. The cost functions considered are the average peak electron density and the rms voltage during the final RF cycle. The simulation is defined to be converged when the average change in the solution values at the middle of the discharge is less than 1×10^{-6} compared to the values in the previous cycle. Using this criteria, it can take more than 250,000 RF cycles to reach full convergence. This is due to the different timescales associated with the species considered in the model. Electrons have very small masses and thus respond quickly to changes in the electric field. This requires one to take a small time step in the simulation. Because of their large masses, the heavier species take many more RF cycles to reach a time-periodic state. These two factors mean that significant computational runtime is required to reach full convergence.

However, it is observed that the cost functions considered obtain a value within 10% of the converged value after 5000 RF cycles. Thus, in the interests of computational efficiency, the simulation is only run for 5000 RF cycles with 400 time steps per cycle (unless otherwise stated). Simulation results were compared for cases that were run with 41, 81, 161 and 321 grid points, and the results showed good agreement. The simulation was run on 4 processors using a Message Passing Interface (MPI) library for communication.

5.1. Verification of derivatives

To verify the accuracy of the sensitivity analysis, sensitivity derivatives are computed using adjoint, direct differentiation, and complex perturbations. In this case, the cost function is defined as the average peak electron density over one RF cycle. The simulation is run with the reaction rate values listed in Table 2, a nitrogen impurity mole fraction of 5×10^{-7}, a gas pressure of 600 Torr, a discharge gap length of 2.4 mm, an rms current density of 21.2 mA/cm^2, a frequency of 13.56 MHz, and a gas temperature of 393 K. Table 5 shows the sensitivity derivatives computed using the adjoint method for all 41 design variables with the peak electron density as the cost function. The derivatives are given using SI units. The derivatives computed using adjoint and direct differentiation differ have relative errors as large as 2.8×10^{-6} and as small as 4.1×10^{-10}, while the derivatives computed using complex perturbations differ from those computed by the adjoint method with relative errors as large as 6.4×10^{-2} and as little as 5.9×10^{-6}.

It is unclear as to the source of the discrepancies between derivatives computed using complex perturbations and those computed using the adjoint method and direct differentiation. Theoretically, these derivatives should match to machine zero precision. Because 5000 cycles are used with 400 time steps per cycle, the simulation is run for a total of 2 million time steps, with several linear solves at each time step. The range of discrepancy corresponds to an average accumulated difference at each time step of between 10^{-8} and 10^{-12}. Unless one obtains an exact linearization for the Jacobian matrix $\frac{\partial \mathbf{R}}{\partial \mathbf{Q}}$, the derivatives computing using differentiation methods will not be accurate. There could possibly be a mistake in the source code that can account for these discrepancies.

5.2. Using sensitivity derivatives to increase a given cost function

Sensitivity derivatives can be used to increase or decrease a cost function. There are many steepest descent or trust region optimization methods that can be used to find a local maximum or minimum. In this case, open source optimization routines

Table 5
Sensitivity derivatives computed using the adjoint method for the average peak electron density.

β	Adjoint derivative	β	Adjoint derivative
k_1	-8.122×10^{30}	l	1.638×10^{19}
k_2	-2.183×10^{27}	j_{rms}	1.002×10^{16}
k_3	7.916×10^{32}	p	6.396×10^{13}
k_4	2.701×10^{29}	f	-1.442×10^{9}
k_5	1.664×10^{34}	T_{gas}	-6.843×10^{13}
k_6	-7.765×10^{27}	μ_e	7.538×10^{17}
k_7	2.007×10^{29}	μ_{He^+}	-2.707×10^{16}
k_8	-2.042×10^{59}	$\mu_{He_2^+}$	-6.132×10^{18}
k_9	-2.257×10^{56}	μ_{N^+}	-1.497×10^{18}
k_{10}	9.288×10^{28}	$\mu_{N_2^+}$	-6.065×10^{17}
k_{11}	9.201×10^{31}	D_e	5.665×10^{17}
k_{12}	-2.574×10^{26}	D_{He^+}	2.279×10^{16}
k_{13}	-1.330×10^{26}	$D_{He_2^+}$	-2.718×10^{18}
k_{14}	-6.428×10^{28}	D_{N^+}	1.797×10^{18}
k_{15}	2.483×10^{29}	$D_{N_2^+}$	-1.807×10^{17}
k_{16}	-2.294×10^{44}	D_{He}	1.226×10^{11}
k_{17}	4.066×10^{26}	D_{He^*}	1.115×10^{17}
k_{18}	-8.101×10^{20}	$D_{He_2^*}$	-7.090×10^{18}
k_{19}	3.624×10^{25}	D_N	-9.768×10^{17}
k_{20}	1.861×10^{22}	D_{N_2}	1.523×10^{19}
f_N	7.676×10^{21}		

[45] which are based on trust region methods are used to vary the physical design variables so as to maximize the peak electron density. Bounds on the physical design variables are put in place so as to prevent arcing, and are based on the parameter range reported in reference [46]. The initial values and bounds are listed below in Table 6.

The simulation is run for 5000 RF cycles using 800 time steps per RF cycle. A smaller time step is used, because the simulation is more sensitive to changes in the physical design variables. The initial peak electron density is found to be $2.02 \times 10^{17}/\text{m}^3$, and after two design cycles, this had increased to its maximum value of $3.28 \times 10^{17}/\text{m}^3$. This maximum value for the peak electron density is found when the discharge gap length, rms current density, and pressure are at the upper bound and when the frequency and gas temperature are at the lower bound.

The results obtained here can be compared to the qualitative study done by Yuan and Raja [11]. They found that as the discharge gap length and rms current density were increased, the peak electron density increased. However, they found that as the pressure was increased, the peak electron density decreased, which is different from the results obtained from the optimizer. It is difficult to say why this discrepancy exists, since very few details were given by Yuan and Raja [11] as to the numerical method that was used and the convergence level that was obtained with their simulation.

5.3. Using sensitivity derivatives to obtain a better estimate for uncertain parameters

It is well known that there is a good degree of uncertainty in the computation of reaction rate coefficients and other parameters used to simulate reaction chemistry [12,47]. Sensitivity derivatives can be used to obtain better estimates of these parameters and coefficients, so that results from computational models more closely match experimental data. This is accomplished by using the reaction rate coefficients and parameters as design variables, and by defining the cost function to be a function that computes the magnitude of the difference between experimental and computational results. The known uncertainty in a given design variable is used to determine the maximum and minimum value of that design variable during the design process. Once the sensitivity derivatives are computed, the design variables are then changed to minimize the cost function.

In this particular case, it is demonstrated how quantitative sensitivity analysis might be used in conjunction with experiments to obtain better estimates for reaction rates. Three experimental data points on a V-I plot are taken from a previous work [48], and the reaction rate coefficients and nitrogen impurity mole fraction are used as design variables. These are

Table 6
Bounds for physical design variables.

Design variable	Initial value	Lower bound	Upper bound
l (m)	2.4×10^{-3}	1.6×10^{-3}	3.2×10^{-3}
j_{rms} (mA/cm^2)	21.2	10.0	30.0
p (Torr)	600	550	650
f (MHz)	13.56	12.0	25.0
T_{gas} (K)	393	250	450

changed during the design process to make the computational data better match the experimental data. The cost function is defined to be

$$I = \sum_{i=1}^{3} (V_{i,e} - V_{i,c})^2, \tag{21}$$

where $V_{i,e}$ is the experimental rms voltage for a given rms current density, and $V_{i,c}$ is the computational rms voltage for a given rms current density. Reducing this cost function will result in improving the agreement between the computational data and the experimental data.

Because cross-section data often has a 50% uncertainty associated with it [47], the reaction rates and transport parameters are bounded between 50% and 150% of the values in Table 2. The nitrogen mole impurity fraction is bounded between 5×10^{-11} and 5×10^{-6}, which is consistent with the experimental data [48]. Twenty-five design cycles using the adjoint method are run for 5000 RF cycles at 400 time steps per cycle on a grid with 81 points. During each design cycle, multiple function evaluations could be called, resulting in a total of 45 function evaluations. The reduction of the cost function is shown below in Fig. 2. A comparison of the voltage–current plots at different points in the optimization routine with the target voltage–current plot is shown in Fig. 3.

The cost function is reduced from 3102 to 188 over the twenty-five design cycles. One can see that the computational data is changed to provide a much better fit to the experimental data. However, there is still some deviation from the experimental data. There are several possible reasons for this. First of all, the design variables were bounded between 50% and 150% of their original values. It is quite possible that these bounds could be expanded, and that doing so would get a closer fit on the V-I plot. Second, there are numerous parameters in the simulation whose sensitivities are not computed, namely the numerical coefficients for powers and exponents of the electron temperature shown in Table 2 that are used to compute reaction rates for chemical reactions. Using these parameters as sensitivity derivatives could result in a better fit on the V-I plot. Third, the chemistry model used in the simulation may be incomplete. Because a fluid model was used for the simulation, a Maxwellian distribution for the electrons was assumed, which is not always valid for a plasma discharge. In addition, there may be certain species or reactions that are not included and would have a significant effect on the V-I profile.

In spite of the deviations from the experimental data, it is clear that the final fit is much better than the initial fit. It is of interest to determine which parameters were most important in reducing the cost function. One can see that by the twentieth function evaluation, the cost function has been reduced by 87.6%. At this point, those design variables which had changed by more than 10% from their initial values were determined to be significant in reducing the cost function. These design variables were $D_e, D_{He_2^*}, D_{N_2}, \mu_e, \mu_{He_2^+}, \mu_{N_2^+}, k_1, k_3, k_{11}$ and f_N. The evolution of the values of these design variables relative to their initial values are plotted in Figs. 4–6. One could conclude that using lower values for $k_1, D_{He_2^*}, D_{N_2}, \mu_e$, and $\mu_{He_2^+}$, and using higher values for $D_e, \mu_{N_2^+}, k_3, k_{11}$ and f_N might be more accurate for this particular simulation.

The final values for each design variable relative to the initial values are shown in Table 7. At the conclusion of the design process, the majority of the design variables are at the limit imposed by the bound constraints.

5.4. Using sensitivity derivatives to compute a bound on computational error

Sensitivity derivatives can be used to assess the effects of uncertainties in input data on the resulting output from a computational model. Reaction rate coefficients and parameters, mobilities, diffusion coefficients and physical parameters (e.g.

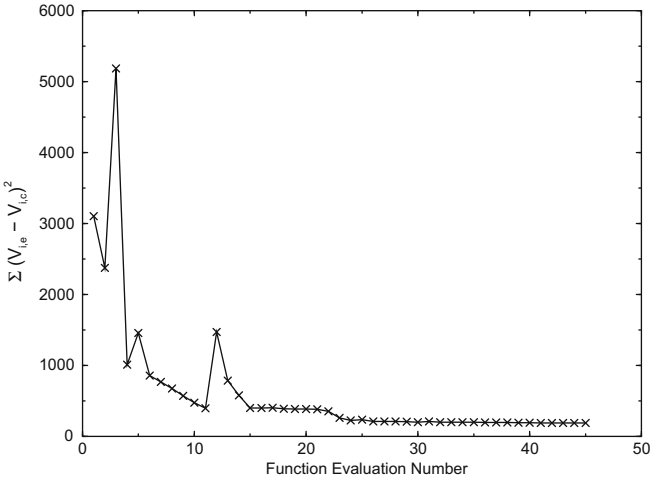

Fig. 2. Cost function reduction over twenty-five design cycles.

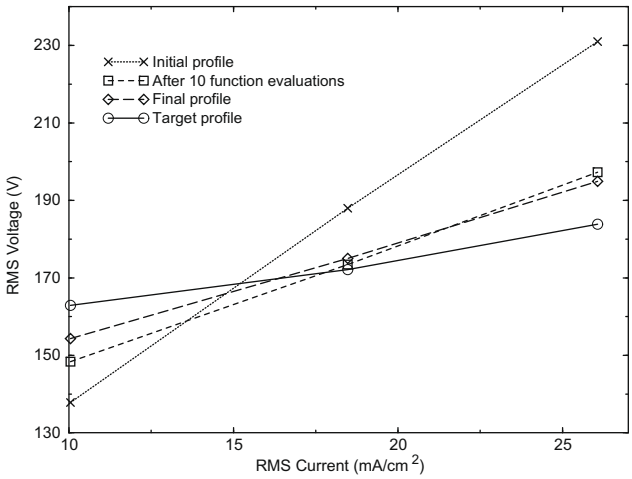

Fig. 3. Voltage–current profiles in optimization routine compared to target voltage–current profile.

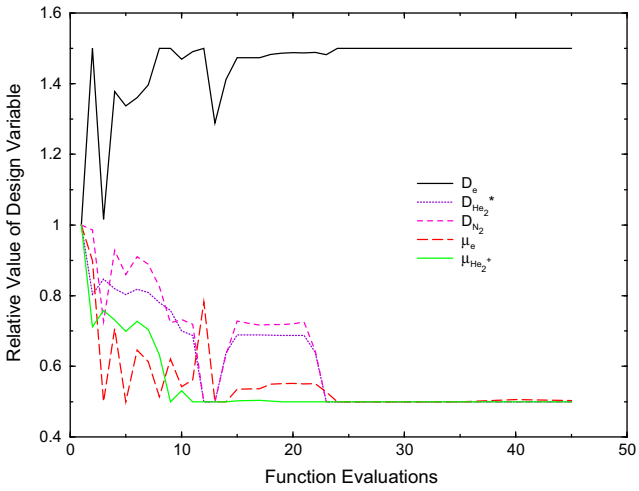

Fig. 4. Evolution of critical design variables in reducing the cost function.

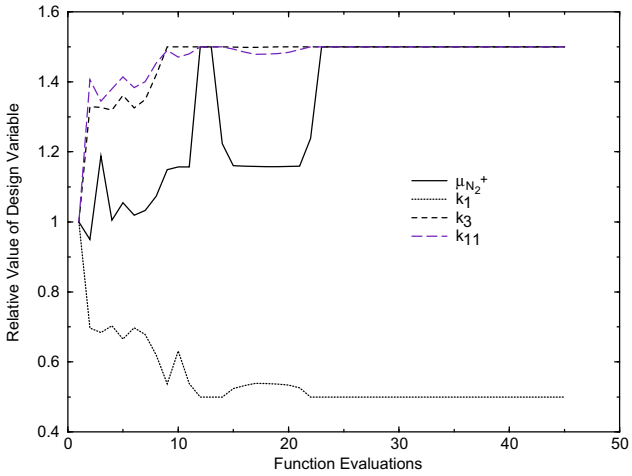

Fig. 5. Evolution of critical design variables in reducing the cost function.

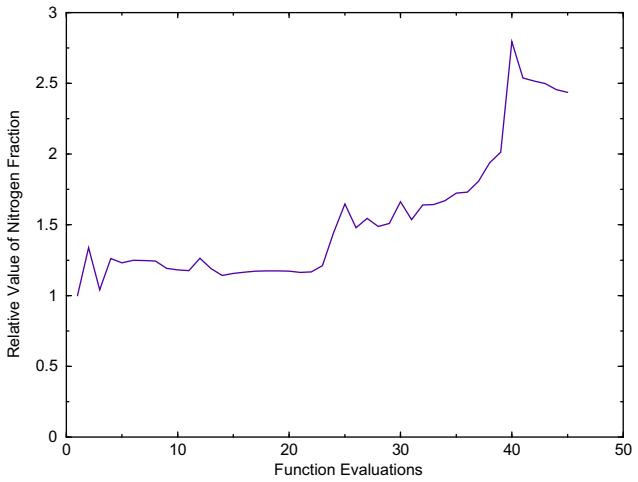

Fig. 6. Evolution of nitrogen fraction in reducing the cost function.

Table 7
Final values for design variables relative to initial values.

Design variable	Final value	Design variable	Final value
k_1	0.500	k_{19}	0.500
k_2	1.500	k_{20}	1.500
k_3	1.500	f_N	2.436
k_4	1.500	μ_e	0.503
k_5	1.312	μ_{He^+}	0.500
k_6	0.500	$\mu_{He_2^+}$	0.500
k_7	1.500	μ_{N^+}	1.500
k_8	0.500	$\mu_{N_2^+}$	1.500
k_9	0.500	D_e	1.500
k_{10}	1.500	D_{He^+}	1.500
k_{11}	1.500	$D_{He_2^+}$	0.500
k_{12}	0.500	D_{N^+}	0.500
k_{13}	0.500	$D_{N_2^+}$	0.500
k_{14}	1.500	D_{He}	1.500
k_{15}	1.500	D_{He^*}	0.500
k_{16}	0.500	$D_{He_2^*}$	0.500
k_{17}	1.500	D_N	0.500
k_{18}	0.500	D_{N_2}	0.500

gas temperature, pressure) all have an associated uncertainty with them. Sensitivity analysis can be used to compute a maximum bound on computational uncertainty for a given cost function. This has been done previously in various fields [49–51].

For a given cost function I, with n_d design variables, the maximum bound on computational uncertainty can be computed as

$$\max|\widehat{I} - I| = \max|\Delta I^g| = \sum_{i=1}^{n_d} \left| \frac{dI^g}{d\beta_n} \Delta\beta_i \right|, \tag{22}$$

where $\Delta\beta_i$ is the known physical uncertainty in design variable i. To get an accurate measure of the upper bound on the uncertainty in this simulation one must obtain sensitivity derivatives and uncertainties for 57 parameters. Many of the uncertainties in these parameters were not reported in the literature, and thus no bound on the uncertainty was computed. However, with the knowledge of all uncertainties, this could be a useful tool for determining the maximum uncertainty of a simulation. It should be noted that this analysis shows determines bounds on the results obtained from the computational model but does not provide a measure of the quality of the model itself.

5.5. Future work

For planned extensions to multiple spatial dimensions, it will be necessary to use Poisson's equation in place of the current conservation equation. The convergence of the computational model will need to be accelerated. There are several

approaches that could be used for this. Some authors have used different time steps for the electrons and the ions, due to their disparate characteristic time scales [3,7]. Other authors have directly solved for the periodic solution of the discharge [52]. Related to the issue of efficiency is the issue of disk storage. Using adjoint for the current problem, it requires the storage of 93 GB of memory. Extending this problem to multiple dimensions will increase these memory requirements even further.

6. Summary

Sensitivity derivatives are computed for a one-dimensional simulation of a high-pressure helium glow discharge. The computed derivatives show good agreement between complex perturbations, direct differentiation, and adjoint. Several applications for quantitative sensitivity analysis are presented. Sensitivity derivatives can be used to increase or decrease a given cost function, to obtain better estimates of uncertain parameters, and to compute a maximum bound on computational uncertainty.

Acknowledgments

Funding for this research has been provided by the Tennessee Higher Education Commission.

References

[1] D. Graves, K. Jensen, A continuum model of dc and rf discharges, IEEE Trans. Plasma Sci. PS 14 (1986) 78–91.
[2] E. Gogolides, H. Sawin, Continuum modeling of radio-frequency glow discharges I. Theory and results for electropositive and electronegative gases, J. Appl. Phys. 72 (1992) 3971–3987.
[3] T. Nitschke, D. Graves, A comparison of particle in cell and fluid model simulations of low-pressure radio frequency discharges, J. Appl. Phys. 76 (10) (1994) 5646–5660.
[4] T.R. Govindan, M. Meyyappan, One-dimensional modeling studies of the gaseous electronics conference rf reference cell, J. Res. Nat. Inst. Stand. Technol. 100 (1995) 463–472.
[5] D. Lymberopoulos, D. Economou, Two-dimensional self-consistent radio frequency plasma simulations relevant to the gaseous electronics conference rf reference cell, J. Res. Nat. Inst. Stand. Technol. 100 (4) (1995) 473–494.
[6] S. Rauf, M. Kushner, Dynamics of a coplanar-electrode plasma display panel cell. I. Basic operation, J. Appl. Phys. 85 (1999) 3460–3469.
[7] E. Hammond, K. Mahesh, P. Moin, A numerical method to simulate radio-frequency plasma discharges, J. Comp. Phys. 176 (2002) 402–429.
[8] Q. Wang, D. Economou, V. Donnelly, Simulation of a direct current microplasma discharge in helium at atmospheric pressure, J. Appl. Phys. 100 (2006) 023301.
[9] E. Gogolides, H. Sawin, Continuum modeling of radio-frequency glow discharges. II. Parametric studies and sensitivity analysis, J. Appl. Phys. 72 (1992) 3988–4002.
[10] S. Rauf, M. Kushner, Dynamics of a coplanar-electrode plasma display panel cell. II. Cell optimization, J. Appl. Phys. 85 (1999) 3470–3476.
[11] X. Yuan, L. Raja, Computational study of capacitively coupled high-pressure glow discharges in helium, IEEE Trans. Plasma Sci. 31 (2003) 495–503.
[12] D. Bose, M. Rao, T. Govindan, M. Meyyappan, Uncertainty and sensitivity analysis of gas-phase chemistry in a chf_3 plasma, Plasma Sources Sci. Technol. 12 (2003) 225–234.
[13] H.-J. Kim, C. Kim, O.H. Rho, Flow control using unsteady aerodynamic sensitivity analysis, in: Proceedings of the AIAA 38th Aerospace Sciences Meeting and Exhibit, AIAA-2000-0515, Reno, NV, 2000.
[14] S. Nadarajah, A. Jameson, Optimal control of unsteady flows using a time accurate method, in: Proceedings of Nineth AIAA/ISSMO Symposium on MAO Conference, AIAA paper 2002-5436, Reno, NV, 2002.
[15] K. Ghayour, O. Baysal, Limit-cycle shape optimization using time-dependent transonic equation, in: Proceedings of 14th Computational Fluid Dynamics Conference, AIAA 1999-3375, Norfolk, VA, 1999.
[16] K. Mani, D. Mavriplis, An unsteady discrete adjoint formulation for two-dimensional flow problems with deforming meshes, in: Proceedings of 45th AIAA Aerospace Science Meeting and Exhibit, 2007.
[17] K. Lange, W.K. Anderson, Sensitivity derivatives for plasma discharge simulations, AIAA J. 47 (6) (2009) 1549–1557.
[18] S. Kanazawa, M. Kogoma, T. Moriwaki, S. Okazaki, Stable glow plasma at atmospheric pressure, J. Phys. D: Appl. Phys. 21 (1988) 838–840.
[19] J. Jeong, S. Babayan, A. Schutze, V. Tu, J. Park, I. Henins, R. Hicks, G. Selwyn, Etching materials with an atmospheric-pressure plasma jet, Plasma Sources Sci. Technol. 7 (1993) 282–285.
[20] H. Herrmann, I. Henins, J. Park, G. Selwyn, Decontamination of chemical and biological warfare (cbw) agents using an atmospheric pressure plasma jet (appj), Phys. Plasmas 6 (5) (1999) 2284–2289.
[21] R. Sladek, E. Stoffels, R. Walraven, P. Tielbeek, R. Koolhoven, Plasma treatment of dental cavities: a feasibility study, IEEE Trans. Plasma Sci. 32 (4) (2004) 1540–1543.
[22] K. Kelly-Wintenberg, D. Sherman, P. Tsai, R. Ben Gadri, F. Karakaya, Z. Chen, J. Roth, T. Montie, Air filter sterilization using a one atmosphere uniform glow discharge plasma (the volfilter), IEEE Trans. Plasma Sci. 28 (1) (2000) 64–71.
[23] J. Roth, D. Sherman, R. Ben Gadri, F. Karakaya, Z. Chen, T. Montie, K. Kelly-Wintenberg, P. Tsai, A remote exposure reactor (rer) for plasma processing and sterilization by plasma active species at one atmosphere, IEEE Trans. Plasma Sci. 28 (1) (2000) 56–63.
[24] Y.P. Raizer, Gas Discharge Physics, Springer-Verlag, New York, NY, 1991.
[25] H. Ellis, R. Pai, E. McDaniel, E. Mason, L. Viehland, Transport properties of gaseous ions over a wide energy range, At. Data Nucl. Data Tables 17 (1976) 177–210.
[26] R. Kee, G. Dixon-Lewis, J. Warnatz, M. Coltrin, J. Miller, A fortran computer code package of gas-phase multicomponent transport properties, Technical Report, SAND86-8246, Sandia National Lab, Livermore, CA, 1995.
[27] J. Shon, M. Kushner, Excitation mechanism and gain modeling of the high-pressure atomic ar laser in he/ar mixtures, J. Appl. Phys. 75 (1994) 1883–1890.
[28] T. Sommerer, M. Kushner, Numerical investigation of the kinetics and chemistry of rf glow discharge plasmas sustained in He, n_2, o_2, He/n_2/o_2, He/cf_4/o_2 and sih_4/nh_3 using a monte carlo-fluid hybrid model, J. Appl. Phys. 71 (1992) 1654–1673.
[29] C. Laux, L. Yu, D. Packan, R. Gessman, L. Pierrot, C. Kruger, R. Zare, Ionization mechanisms in two-temperature air plasmas, in: Proceedings of 30th AIAA Plasmadynamics and Lasers Conference, AIAA 99-3476, Norfolk, VA, 1999.
[30] K. Lange, A fully implicit characteristic-based algorithm for a one-dimensional radio frequency glow discharge fluid simulation, Master's thesis, The University of Tennessee at Chattanooga, July 2007.

[31] Y. Saad, M. Schultz, Gmres: a generalized minimal residual algorithm for solving nonsymmetric linear systems, SIAM J. Sci. Statist. Comput. 7 (1986) 856–869.
[32] O. Axelsson, Iterative Solution Methods, Cambridge University Press, 1994.
[33] J. Newman, W. Anderson, D. Whitfield, Multidisciplinary sensitivity derivatives using complex variables, Technical Report, MSSU-EIRS-ERC-98-08, Mississippi State University, Mississippi State, MS, 1998.
[34] W. Anderson, J. Newman, D. Whitfield, E. Nielsen, Sensitivity analysis for the navier-stokes equations on unstructured meshes using complex variables, in: Proceedings of 14th Computational Fluid Dynamics Conference, AIAA 1999-3294, Norfolk, VA, 1999.
[35] J. Newman, W. Anderson, D. Whitfield, E. Nielsen, Step-size independent approach for multidisciplinary sensitivity analysis, J. Aircraft 40 (3) (2003) 566–573.
[36] G.J.-W. Hou, A.I. Taylor, V. Korivi, Discrete shape sensitivity equations for aerodynamic problems, in: Proceedings of the 27th AIAA/SAE/ASME/ASEE Joint Propulsion Conference, AIAA-91-2259, Sacramento, CA, 1991.
[37] O. Pironneau, On optimum design in fluid mechanics, J. Fluid Mech. 64 (1974) 97–110.
[38] A. Jameson, Aerodynamic design via control theory, J. Sci. Comp. 3 (1988) 233–260.
[39] A.I. Taylor, G. Hou, V. Korivi, Methodology for calculating aerodynamic sensitivity derivatives, AIAA J. 30 (10) (1992) 2411–2419.
[40] S. Ta'asan, G. Kuruvila, M. Salas, Aerodynamic design and optimization in one shot, in: Proceedings of 30th Aerospace Science Meeting, AIAA-92-0025, Reno, NV, 1992.
[41] W. Anderson, V. Venkatakrishnan, Aerodynamic design optimization on unstructured grids with a continuous adjoint formulation, Comput. Fluids 28 (4–5) (1999) 443–480.
[42] J. Elliott, J. Peraire, Practical three-dimensional aerodynamic design and optimization, AIAA J. 35 (9) (1997) 1479–1485.
[43] E. Nielsen, W. Anderson, Aerodynamic design optimization on unstructured meshes using the Navier–Stokes equations, AIAA J. 37 (11) (1999) 957–964.
[44] S. Nadarajah, A. Jameson, A comparison of the continuous and discrete adjoint approach to automatic aerodynamic optimization, in: Proceedings of AIAA 38th Aerospace Science Meeting and Exhibit, AIAA-2000-0667, Reno, NV, 2000.
[45] J. Dennis, D. Gay, R. Welsch, Algorithm 573: an adaptive nonlinear least-squares algorithm, ACM Trans. Math. Software 7 (3) (1981) 367–383.
[46] J. Park, I. Henins, H. Herrman, G. Selwyn, Discharge phenomena an atmospheric pressure radio-frequency capacitive plasma source, J. Appl. Phys. 89 (1) (2001) 20–28.
[47] W. Janev, K.J. Langer, D.J. Post, Elementary Processes in Hydrogen–Helium Plasmas, Springer, Berlin, 1987.
[48] J. Park, I. Henins, G. Selwyn, Gas breakdown in an atmospheric pressure radio-frequency capacitive plasma source, J. Appl. Phys. 89 (1) (2001) 15–19.
[49] B. Blackwell, K. Dowding, R. Cochran, D. Dobranich, Utilization of sensitivity coefficients to guide the design of a thermal battery, in: Proceedings of 1998 ASME International Mechanical. Engineering Congress and Exposition, vol. 361, Anaheim, CA, 1998, pp. 73–82.
[50] M. Putko, P. Newman, A. Taylor III, L. Green, Approach for uncertainty propagation and robust design in cfd using sensitivity derivatives, in: Proceedings of 15th AIAA Computational Fluid Dynamics Conference, AIAA 2001-2528, Anaheim, CA, 2001.
[51] E. Turgeon, D. Pelletier, S. Etienne, J. Borggaard, Sensitivity and uncertainty analysis for turbulent flows, in: Proceedings of 40th AIAA Aerospace Science Meeting and Exhibit, AIAA 2002-0985, Reno, NV, 2002.
[52] E. Gogolides, H. Sawin, R. Brown, Direct calculation of time-periodic states of continuum models of radio-frequency plasmas, Chem. Eng. Sci. 47 (1992) 3839–3855.